Journal of Environmental Chemical Engineering 9 (2021) 105069

Contents lists available at ScienceDirect

Journal of Environmental Chemical Engineering

journal homepage: www.elsevier.com/locate/jece

Degradation behavior of mixed and isolated aromatic ring containing VOCs: Langmuir-Hinshelwood kinetics, photodegradation, in-situ FTIR and DFT studies

Asad Mahmood *, Xiao Wang, Xiaofeng Xie, Jing Sun *

State Key Laboratory of High-Performance Ceramics and Superfine Microstructure Shanghai Institute of Ceramics, Chinese Academy of Sciences, 1295 Dingxi Road, Shanghai, China

ARTICLE INFO

Editor: Dr. G. Palmisano

Keywords:
VOCs
TiO_2
Photocatalysis
DFT
In-situ FTIR

ABSTRACT

The photodegradation tendencies of mixed and isolated VOCs, e.g., benzene, toluene, and *p*-xylene were studied using TiO_2 P25 as a model photocatalyst. The degradation of VOCs in the mixture is significantly affected by the existence of different organic pollutants. For example, benzene only showed 10% degradation efficiency in the mixture whilst 67% in the isolated mode. The conversion efficiency of benzene was 20% and 27% when mixed with *p*-xylene and toluene, respectively. It shows that the degradability of benzene is influenced more by the presence of *p*-xylene than toluene. The dynamic adsorption-desorption experiments and DFT calculations on stoichiometric and defective TiO_2 surface revealed that benzene only weakly interacts with the stoichiometric TiO_2 surface than toluene and *p*-xylene. This behavior could be the fundamental factor for the lower degradation efficiency of benzene. Furthermore, the presence of oxygen vacancy (O_v) in TiO_2 surface tremendously improved the overall adsorption of VOCs. Several Langmuir-Hinshelwood kinetic models, which are based on different reaction dynamic assumptions, were used to determine rates of reactions, water adsorption equilibrium constant, and VOCs adsorption equilibrium constant. The results indicated that the oxidation of VOCs occurred on the catalyst surface, and the adsorption equilibrium constant of VOCs was higher than water adsorption equilibrium constant. The intermediate formation and hydroxyl groups consumption were further rationalized via in-situ FTIR study. This work provides a comprehensive analysis of VOCs degradation in the mixed and isolated mode, which will increase the possibility of implementing the photocatalytic oxidation technology for the VOCs abatement.

1. Introduction

As a result of urbanization and rapid industrial expansion, a majority of people today spent much of their time indoors [1]. It is well thought out how the indoors air environment is much polluted than the outdoors [2]. The air environment is mostly contaminated by the inclusion of low boiling point (≤250 °C) organic pollutants termed as volatile organic compounds (VOCs) [3,4,5]. These VOCs are accountable for the depletion of ozone (O_3) and also aid to secondary organic aerosol (SOA) formation, when oxidized by Cl, •OH radicals, O_3, and NO_3 radicals. A long-term exposure to VOCs can potentially cause some severe health problems and can also cause terminal ailments. Thus, quite a few technologies have already been developed, which integrate thermal catalysis, microbial degradation, plasma assisted degradation, and photocatalytic oxidation to get rid of VOCs in the indoors as well as the outdoors environment [6,7,8].

Among these, the photocatalytic oxidation technology (PCO) has been thoroughly researched for the VOCs abatement [9,10]. This technology makes use of oxide-based semiconductor materials, which generate reactive oxygen species (ROS), i.e., superoxide anion, $\bullet O_2^-$, hydroxyl radical, •OH, and hydrogen peroxide, H_2O_2, at the expense of solar energy, which further participate in the surface catalyzed reactions. Because of these scientific studies, a significant advancement has been made in the PCO technology, both on the material's level as well as engineering perspectives of designing a reactor. The potential of materials to harvest the extended solar spectrum continues to be studied. For example, pristine anatase TiO_2, $E_g = 3.2$ eV, only harvest light in the ultra-violet (UV) region, which entail only < 5% of the solar

* Corresponding authors.
E-mail addresses: amkhan036@yahoo.com (A. Mahmood), jingsun@mail.sic.ac.cn (J. Sun).

https://doi.org/10.1016/j.jece.2021.105069
Received 26 October 2020; Received in revised form 8 January 2021; Accepted 10 January 2021
Available online 13 January 2021
2213-3437/© 2021 Elsevier Ltd. All rights reserved.

spectrum [11]. This implicit optical character impedes the usefulness of pristine TiO_2 in the PCO technology. Thus, to overcome this challenge, impurities (i.e., N_2, B, Cu, etc.) are doped in TiO_2 crystal lattice to modify the optical bandgap [12,13,14]. Likewise, the photoinduced charge recombination mechanism has been extensively studied to create oxide-based semiconductor materials suitable for practical opto-electrical applications [15,16]. Even though, some good results have already been accomplished, most of the studies take into account the destruction of isolated (single mode) VOCs as a model pollutant. The effect of mixture on the conversion efficiency and chemical rate kinetics is generally overlooked [11,17,18,19]. The degradation pathways of mixed VOCs could possibly be different than an isolated mode, which have rarely been studied. Considering that the recent standards [1] provide information regarding the PCO functionality of the major pollutants, no assessment is accessible to compare the degradation rate of mixed and isolated VOCs [20]. Thus, the parameters, which influence the overall performance of photocatalysts, reactor design, and the reaction conditions to realize best possible conversion efficiency are elusive. One such attempt was reported by Liu et al. [18] who examined the simultaneous degradation of toluene and styrene using a non-thermal plasma (NTP) and NTP-catalysis. The study shows that toluene degradation is affected by the existence of styrene in the mixture. Actually, styrene inhibited the degradation of toluene under plasma treatment. On the contrary, styrene would not show any apparent inhibition because of toluene. The in-depth mechanistic study indicated that styrene degradation resulted in benzaldehyde being an intermediate species, which utilized ROS, i.e., $\bullet O_2^-$ and •OH radicals. The intake of active oxide radicals by benzaldehyde largely affected the degradation of toluene, since, a limited number of active oxide radicals are generated. Also, the breaking of C–H bond of methyl ($-CH_3$) group in toluene ($C_6H_5CH_3$) requires high energy electrons than $C^{=}C$ bond breaking of vinyl ($CH_2^{=}CH-$) group in styrene ($C_6H_5CH^{=}CH_2$), which reduces the possibility of toluene degradation. Another factor, which could have influenced the overall degradation is the effective use of ozone. Assessment of final product revealed less ozone content in the case of styrene, which suggested that styrene degradation involved more ozone consumption. In contrast, a large quantity of ozone was detected when toluene was used as a target pollutant, which indicated that less ozone was consumed during toluene degradation. The study highlights that the end group of styrene and toluene were essentially responsible for the initial oxidation mechanism. Debono et al. [21] studied the VOCs, i.e., toluene, decane, and trichloroethylene (TCE) mixture effect at the ppb level. The results revealed a sequential degradation of VOCs guided by the competitive adsorption of different pollutant gases in the mixture. Also, the degradation of a particular pollutant gas was delayed by the mixture effect, however, the mineralization was observed to increase. These attempts provide useful information about the VOCs mixture effect. An essential aspect in gas-solid heterogeneous catalysis will be the interaction of VOCs with the catalyst's surface [19,22]. The adsorption of a pollutant gas and resident time are the critical parameters, which affect the ultimate conversion. Furthermore, the degradation of merely one VOC does not imitate the practical circumstances, considering that the VOCs are typically present in the mixture form, thereby photodegradation could possibly be afflicted with the competitive adsorption of various VOCs, exhibiting distinctive molecular structures and polarity [23,24]. The VOCs are generally degraded through several intermediate steps before mineralized into CO_2 and H_2O [25,26]. The production and stability of intermediate species may also affect the overall degradation reaction, because the intermediate species might cover the active surface sites, which will ultimately impede further reaction. For this reason, it is vital to examine and evaluate the behavior of mixed-VOCs and compare it with their single mode reactions. Also, the kinetic parameters must be thoroughly examined to ascertain an appropriate degradation mechanism, which is essential to illustrate the behavior of pollutant gases in the course of photodegradation.

Considering above, we studied in detail the PCO of aromatic ring containing VOCs, including benzene, toluene, and *p*-xylene on commercial TiO_2 P25 and compared their degradation with an isolated mode of these pollutant gases. To rationalize our experiment, a similar concentration of isolated pollutant gases was used as in a mixture. Three different mixtures were used, which included benzene with toluene and *p*-xylene, benzene with *p*-xylene, and benzene with toluene. The VOCs utilized in these experiments are among the common pollutants, which have attracted immense interest and concern on a global level. These VOCs are delivered through several sources in the atmosphere, e.g., paints, industrial operation and exhausts from vehicles, which poses serious health risks in both humans and animals [27,28]. As anticipated, the degradation efficiency of these pollutant gases was quite different in mixtures compared to their isolated mode. The *p*-xylene exhibited a high photodegradation efficiency both in mixtures as well as in isolated mode. Different kinetic models proposed by Langmuir and Hinshelwood (Langmuir-Hinshelwood; L-H) were used to fit the experimental data [29]. These models revealed useful information about the degradation mechanism of VOCs in different mixtures and in isolated mode. Also, the L-H models highlight the role of water content in the degradation mechanism. The density functional theory (DFT) study revealed that the defective TiO_2 (101) surface is quite active towards the VOCs capture when compared with the stochiometric TiO_2 (101) surface. The in-situ FTIR study further revealed the formation of different intermediated species and their variations (at least formation tendency) in different modes. This study is quite useful to understand the kinetics and degradation mechanism of VOCs on commercial TiO_2 P25, which can be extended to other VOCs and materials.

2. Experimental section

2.1. Materials and processing

Commercial TiO_2 P25 (measured Brunauer–Emmett–Teller; BET; surface area = 27 m^2/g) was received from the Evonik Industries AG. Commercial TiO_2 P25 is composed of both anatase and rutile crystal phases (~80:20 ratio). The as-received TiO_2 P25 powder was washed with deionized water (Milli-Q® type-I water) and absolute ethanol (C_2H_6O, AR, 99.7%, Zhenxing No.1 Chemical Plant), which were dried in an electric furnace at 100 °C before use. The crystallographic structure of TiO_2 P25 sample was studied with powder X-ray diffraction (XRD; Ultima IV 2036E102, Rigaku Corporation, Japan). The XRD analysis confirmed the characteristic anatase and rutile phases in TiO_2 P25 (Fig. S1).

2.2. Photocatalytic tests

The dynamic adsorption-desorption and photodegradation reactions were carried out in an automated gas-flow reaction chamber, whilst the VOCs content was monitored through a coupled GC. The schematic view of the reactor is given in Fig. 1. According to Fig. 1, the air and VOCs from cylindrical containers are allowed to pass through valves 1 and 2, which is subsequently mixed using a mixer. The flow of gases can be adjusted to stabilize the instrument and carry out the adsorption process in the reaction cell. The sample gas is directly passed through the coupled GC by changing the flow direction from valve 3 → 4→ GC. Once the GC signals are stabilized, the flow of sample gases is directed towards the reaction cell by adjusting the sample gas flow direction using valve 3. The outlet gases follow the path; reaction cell → 5 → 4 → GC. All of these valves are adjustable, which can be used to control the flow of sample gases in a desired direction. The concentration of VOCs is determined through an FID detector of GC. In a typical reaction, 0.1 g of TiO_2 P25 powder was dispersed in ethanol (10 mL) and sonicated for 30 min. The well-prepared slurry was drop coated on a glass substrate (dimension: 16 × 13 cm) and dried in an electric oven at 120 °C for 2 h. The catalyst coated substrates were then transferred into the reaction

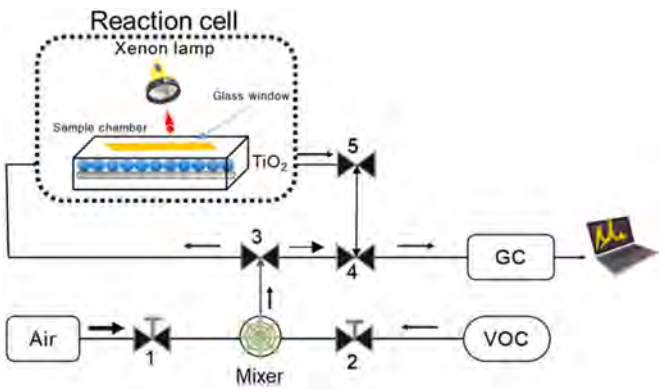

Fig. 1. A schematic view of the dynamic adsorption-desorption and photo-degradation reaction chamber.

cell. The reaction cell comprises a glass window for light irradiation. The distance between the light source and samples was kept constant (30 cm). The adsorption-desorption equilibrium was carried out in the dark. After achieving the adsorption-desorption equilibrium, the samples were irradiated using a 400 W xenon lamp with an illumination density of 80 mW/cm^2 measured with THORLABS GmbH (PM100D; S314C detector) as the radiation source. The mixture of VOCs included benzene (20 ppm), toluene (20 ppm) and *p*-xylene (20 ppm). The flow rate was kept constant in all experiments (20 sccm). The relative humidity (RH = 43%) in the reaction cell was measured using a digital hygrometer. Three different mixtures were tested, such as mixture-A (benzene, toluene, and *p*-xylene), mixture-B (benzene and *p*-xylene), and mixture-C (benzene and toluene). The target VOCs were also used in isolated mode (20 ppm each) to compare their degradation with the mixture. According to these experiments, the conversion efficiency (φ) was calculated; $\varphi = (C_0 - C)/C_0 \times 100\%$, where C_0 and C are the initial and after different time interval concentration of the gas, respectively. After stabilization, before starting the light, when a dynamic adsorption-desorption equilibrium is achieved, the light is turned on. The last stable value before light irradiation is taken as C_0. The concentration progressively decreased, which is determined at different time intervals. This concentration is C.

2.3. Computational details

The density functional theory calculation was performed using *Vienna Ab-initio simulation package* (*VASP*) [30,31,32]. As commercial TiO_2 P25 is composed of rutile and anatase phases, however, the anatase phase exhibit a higher ratio than rutile phase. In this way, pure and defective anatase TiO_2 (101) surface was used to study the adsorption of benzene, toluene and *p*-xylene. The bulk TiO_2 was optimized, which was further cleaved to model TiO_2 (101) surface (2 × 3 × 1 supercell). The supercell contained 108 no. of ions including 72 oxygen and 36 titanium. A vacuum level of 20 Å was used in all calculations. For geometry optimization and properties calculations, generalized gradient approximation (GGA) implemented by Perdew-Burke-Ernzerhof (PBE) was used as an exchange-correlation function [33]. In order to account for the weak Van der Waals forces, a semiempirical dispersion correction (DFT + D) method given by Grimme was used [34]. The slab structure was relaxed using a cutoff energy (E_{cut}) of 520 eV utilizing an ultrafast pseudopotential. The energy convergence and ionic displacement tolerance was 0.1 × 10^{-5} eV/atom and 0.3 × 10^{-1} eV/Å, respectively. To mimic the surface model, the bottom two layers were applied constrains. The *k*-point set 3 × 3 × 1 was sampled using Monkhorst-pack grid along the Brillouin zone. The calculations were performed for the atomic configuration of different atoms as follows: Ti: 3s^2 3p^6 3d^2 4s^2, O: 2s^2 2p^4; H: s^1; C: 2s^2 2p^2. Similar parameters were used for the defective (oxygen vacancy; O_v) surface models, further including dipole correction method. The calculation criteria of rutile TiO_2 (110) surface were kept the same. The adsorption energy (E_{ads}) was calculated for the tested configurations using Eq. (1):

$$\Delta E_{ads} = (E_{Molecule} + E_{Surface}) - E_{Molecule/surface} \quad (1)$$

where $E_{Molecule}$ is the energy of a molecule in the gas phase, $E_{Surface}$ is the slab energy without adsorption and $E_{Molecule/Surface}$ is the energy of the surface and molecule complex.

2.4. In-situ FTIR study

The in-situ DRIFTS experiments were carried out using the FTIR spectrometer (Hitachi Tracer 100 combined with mercury-cadmium-telluride detector) equipped with a temperature control system. The in-situ FTIR study was performed using isolated VOCs and mixture-A (benzene, toluene, *p*-xylene). In the beginning, the sample powder was mounted inside a pellet shaped sample holder (PIKE Technology), which incorporate two KBr windows and a glass window. The sample powder was manually pressed for mechanical stability. The reaction chamber was firmly closed before the reaction. Next, the N_2 gas was flown throw the reaction chamber for 30 min. The temperature of the chamber was raised to 200 °C, which was allowed to stay there for 1 h. The chamber was cooled down to room temperature prior to allowing the pollutant gas to flow through the reaction chamber. The target VOCs was allowed to flow through the reaction chamber for 1 h. Once the final absorption spectra were attained, the VOCs supply was switched off. A xenon light with an intensity of 500 W was used during the photodegradation reaction. The last absorption spectrum of the adsorption process was deducted from the spectra collected during the degradation process, which were attained under light irradiation. In this manner, we were able to achieve more pronounced peaks of the new species appeared on the catalyst's surface/reaction chamber. The FTIR spectra were automatically collected at 3 min time interval.

3. Results and discussion

3.1. photodegradation of VOCs

Fig. 2 shows the degradation of VOCs in the mixture-A and their single mode under light illumination. In mixture-A, benzene demonstrated a poor degradation efficiency (10%) (Fig. 2a) in contrast to toluene (52%) (Fig. 2b) and *p*-xylene (91%) (Fig. 2c). When benzene was used as the only pollutant gas in the degradation reaction, a 67% of degradation efficiency was achieved. A significant increase in the degradation efficiency of toluene and *p*-xylene was also recorded in isolated mode. For instance, 100% toluene was degraded in isolated mode. The *p*-xylene was completely degraded in less time when used as a single pollutant gas. This behavior might be associated with various factors. It is well thought out that the gas-solid reactions are quite different from the solution phase. In solutions based photocatalytic reactions, the electron transfer might occur through the electrolyte. Also, the intermediate formed on a photocatalyst surface could possibly be removed through the Brownian motion of the electrolyte molecules. However, in gas-solid reactions, the interaction between the pollutant molecules and a catalyst surface is critical. The gas molecules are first adsorbed on a catalyst surface, which either directly react with the photoinduced holes, or react with the reactive oxygen species on the surface, e.g., $\bullet O_2^-$ and •OH radicals [35]. The interaction of gas molecules with a catalyst surface is influenced by molecular structure and polarity of molecules as well as the atomic arraignment of catalyst's surface [36,37]. Thus, it can be inferred that benzene poorly interacted with TiO_2 P25 when toluene and *p*-xylene were present in the mixture-A. Similarly, the toluene molecules, which contains one $-CH_3$ group attached to the aromatic ring, more weakly interacted than *p*-xylene molecules (two $-CH_3$ groups/aromatic ring). The DFT calculation was

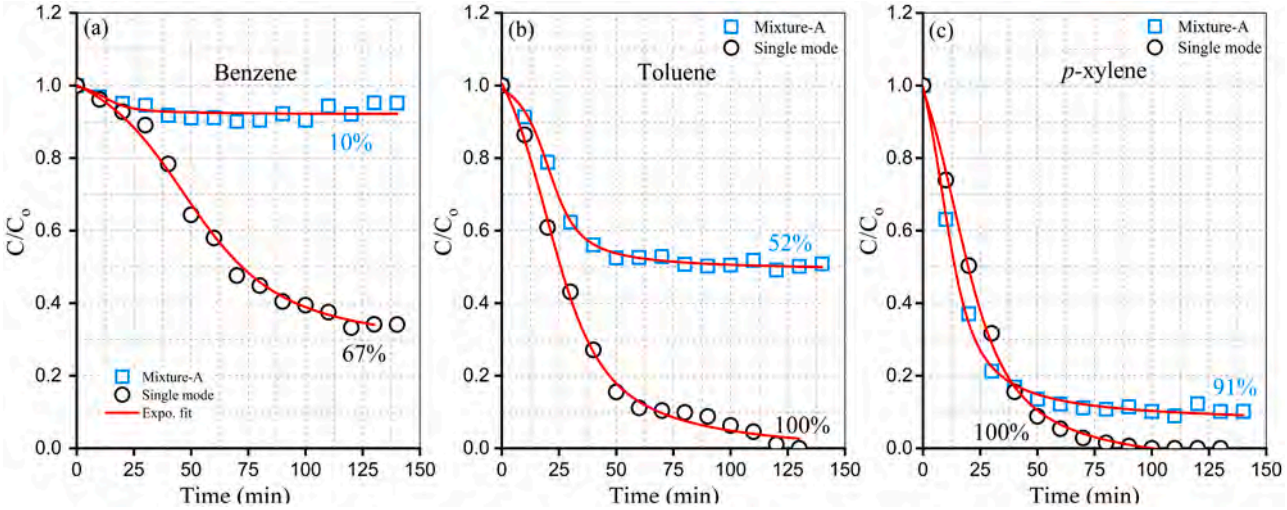

Fig. 2. Photodegradation of VOCs in the mixture-A and isolated mode under UV–vis light irradiation.

carried out to understand the adsorption behavior of these VOCs on TiO_2 surface. Initially, we studied the adsorption of VOCs on stoichiometric anatase TiO_2 (101) surface (Fig. 3). It can be seen that all of the molecules configured to almost the same geometry on stoichiometric TiO_2 (101) surface, forming a 26° orientation along the Ti–O–Ti layer relative to the imaginary surface plane. The toluene and *p*-xylene demonstrated somewhat similar behavior. The adsorption energy value of benzene (E_{ads} = 0.541 eV) is smaller than toluene (0.597 eV) and *p*-xylene (0.767 eV) on stoichiometric TiO_2 (101) surface. These values suggest that *p*-xylene strongly adsorb on TiO_2 (101) surface in comparison to benzene and toluene, which could be associated with the high degradation efficiency of *p*-xylene. The dynamic adsorption-desorption curves for mixture-A, -B, and -C also confirmed this behavior (Fig. S2 and S3). In mixture-A and isolated mode, *p*-xylene exhibited a large adsorption curve area in comparison to the blank chamber (Fig. S2a and Fig. S2b). Also, the adsorption curve area of *p*-xylene (mixture-B) and toluene (mixture-C) is greater than benzene, which further confirmed weak interaction of benzene with TiO_2 P25 surface (Fig. S3). Another factor could be the availability of active species of a catalyst surface. For example, under given circumstances, the large number of reactive species is consumed by *p*-xylene and the intermediates formed as a result of *p*-xylene degradation. This could cause a decrease in the number of reactive species available for toluene and benzene (detail is given in in-situ FTIR section). The adsorption behavior can be further seen in the electron density difference. The blue region depicts the electron rich region while the yellow region is the electron depleting region. It can be noted that the VOCs molecules adsorb on TiO_2 (101) surface by configuring the aromatic ring parallel to the adsorption site. Also, more

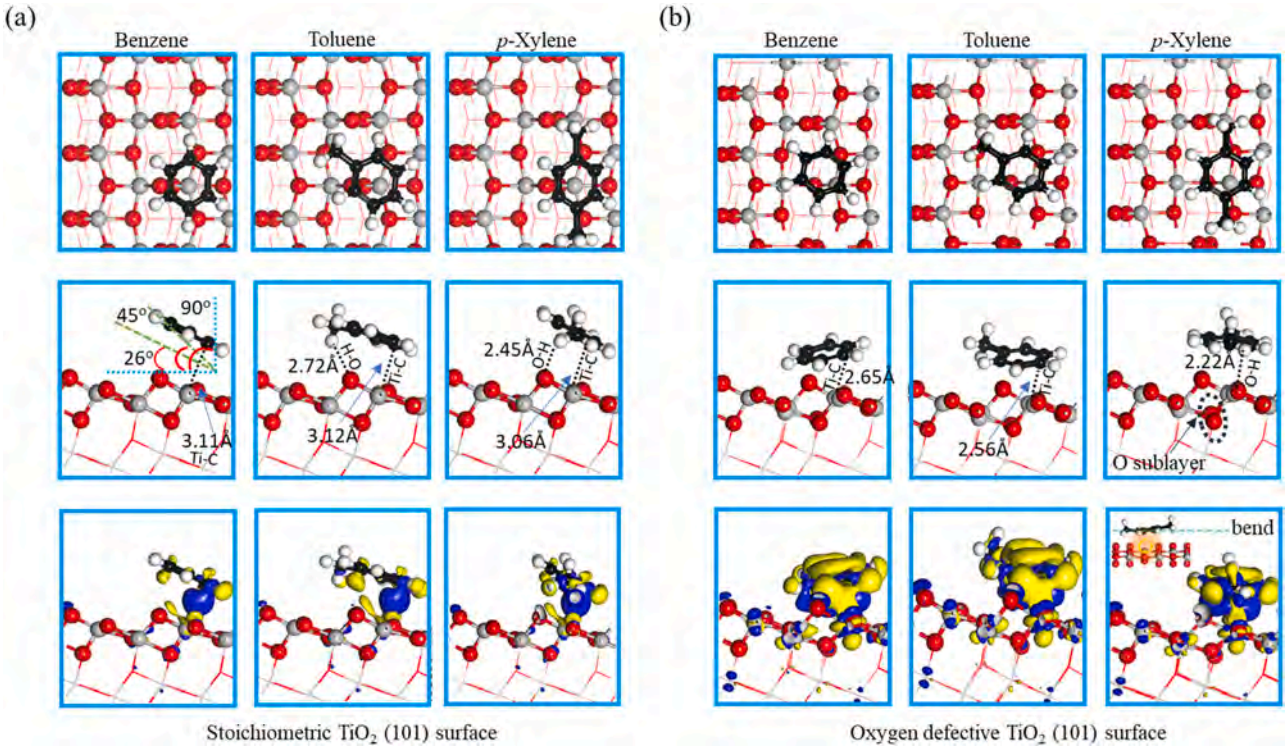

Fig. 3. Stable adsorption configuration of benzene, toluene, and *p*-xylene on stochiometric and defective TiO_2 (101) surface. The shortest atomic distance between the surface and VOCs molecules is given in Å.

electron density is shared between the molecule and surface in the case of toluene and *p*-xylene than benzene (Isovalue = 0.005), which further confirmed the poor interaction of benzene. Next, we carried out similar DFT calculations for the defective TiO_2 (101) surface using an oxygen vacancy. The presence of an oxygen vacancy on TiO_2 (101) facilitated the adsorption of VOCs, which showed a high adsorption energy than ideal TiO_2 (101) surface. The adsorption energy of benzene, toluene, and *p*-xylene on defective TiO_2 (101) surface was calculated as 0.912 eV, 1.0 eV, 1.09 eV, respectively. These results suggested that the VOCs will interact more strongly with oxygen vacancy sites through the π-electrons of an aromatic ring, which will further improve the reactivity of the surface and molecules. As, the TiO_2 P25 contains a small percentage (~20) of rutile phase, thus, we also tested the adsorption of target VOCs on rutile TiO_2 (110) surface (Fig. S4). The target VOCs exhibited the same behavior on rutile TiO_2 (110) surface. The E_{ads} values for benzene, toluene, and *p*-xylene on rutile TiO_2 (110) surface are 0.248 eV, 0.457 eV, and 0.502 eV, respectively. It can be concluded that the aromatic ring containing VOCs, benzene, toluene, and *p*-xylene, interact through theirs π-electrons of the aromatic rings. The molecules interact strongly with the defective TiO_2 (101) surface than ideal surface.

We further studied the degradation behavior of benzene with *p*-xylene (mixture-B) and toluene (mixture-C) (Fig. 4). When *p*-xylene was used with benzene, a 20% of benzene was degraded, while 93% of conversion efficiency was achieved for *p*-xylene (Fig. 4a, b). When toluene was mixed with benzene, a 27% of degradation was achieved while toluene showed 80% degradation efficiency (Fig. 4c, d). When we compare the degradation tendencies of target VOCs in all of these mixtures, it is obvious, that the degradation of benzene is comparatively less affected by toluene while more affected by *p*-xylene in the respective mixtures. This behavior might be associated with the strong interaction of *p*-xylene with the catalyst surface than toluene and benzene.

3.2. Kinetic study

To study the kinetics of aromatic ring containing VOCs, the Langmuir-Hinshelwood (L-H) kinetic models were applied to the degradation data of different mixtures (i.e., A, B, and C) and VOCs in the single mode. The L-H models have been widely used for the gas-solid reactions [29,38]. The experimental oxidation rate for different cases in our study was calculated using the following equation.

$$-r = \frac{F}{V}Xi = \frac{F}{V}\left(\frac{C_{in} - C_{out}}{C_{in}}\right) \quad (2)$$

where r is the reaction rate of different VOCs (ppmv min^{-1}), *F* is the flow rate, *V* is the volume of the chamber (320 mL), C_{in} and C_{out} are the inlet and outlet concentration of VOCs. To fully understand the nature of our data, we applied seven different models given in Table 1. These models are based on different assumptions, which determine the behavior of VOCs, absence/presence of moisture and reaction dynamics. The non-linear least square regression analysis was used to fit these models to experimental data in order to determine different parameters including rate constant, *k*, adsorption equilibrium constant of VOCs, K_A, and adsorption equilibrium constant of water, K_W. The suitability of the models was estimated based on the residual sum of squares ($RSS = \sum(R_{pred} - R_{exper})^2$) and R-squared ($R^2$) values.

Different parameters based on model-1 is given in Table 2, which assume that the water content does not contribute to the oxidation reaction of VOCs. It can be seen that in the mixture-A, *p*-xylene exhibit a

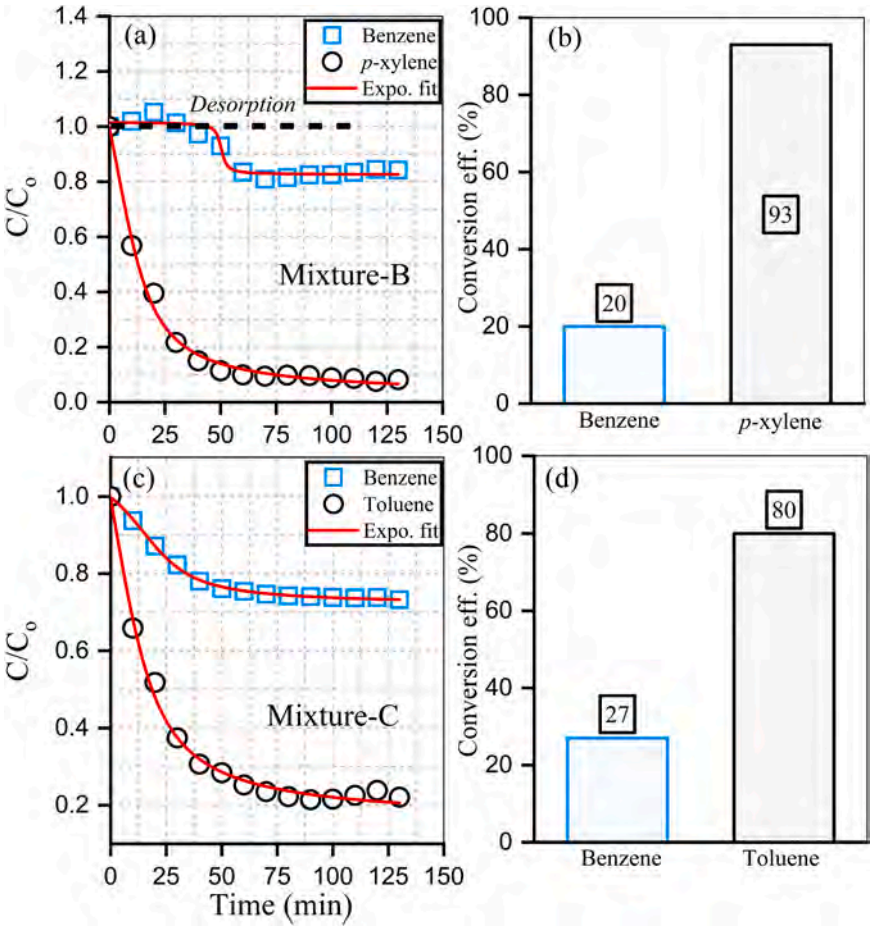

Fig. 4. Photodegradation of VOCs in the mixture-B and mixture-C and isolated mode under UV–vis light irradiation.

Table 1
The rate expressions applied to experiments with and without water.

Model	Kinetic rate expression	Assumption
1	$-r = k \times \frac{K_A C_A}{1 + K_A C_A}$	Reaction of VOCs adsorbed on catalyst surface but water does not take part in the reaction.
2	$-r = k \times \frac{K_A C_A K_W C_W}{1 + K_A C_A}$	Reaction of VOCs adsorbed on catalyst surface and react with water.
3	$-r = k \times \frac{K_A C_A}{(1 - K_A C_A + K_W C_W)}$	VOCs and water adsorbed on catalyst surface but water does not take part in the reaction.
4	$-r = k \times \frac{K_A C_A K_W C_W}{(1 + K_A C_A + K_W C_W)}$	Reaction of VOCs and water adsorbed on catalyst surface.
5	$-r = k \times \frac{K_A C_A}{(1 + K_A C_A)} + \frac{K_W C_W}{(1 + K_W C_W)}$	Reaction of VOCs and water adsorbed on different active sites.
6	$-r = k \times \frac{K_A C_A K_W C_W}{(1 + K_W C_W)}$	Reaction of water adsorbed on catalyst surface and gas-phase VOCs.
7	$-r = k \times \frac{(K_A C_A K_W C_W)^{1/2}}{[1 + (K_A C_A)^{1/2} + (K_W C_W)^{1/2}]^2}$	Reaction of VOCs and water dissociatively adsorbed on catalyst surface.

high k value (0.0634 ppmv min^{-1}) in contrast to benzene (0.0095 ppmv min^{-1}) and toluene (0.0392 ppmv min^{-1}). Also, the K_A of *p*-xylene is higher than benzene and toluene, which suggested that *p*-xylene easily adsorbed on the catalyst surface in contrast to other aromatic ring containing VOCs. The k increased for the VOCs in isolated mode in contrast to the mixture-A while the K_A decreased. A similar pattern was observed in the mixture-B and mixture-C, where benzene showed a small value of k. To further understand the role of moisture in the oxidation reaction, non-linear multiple regression analysis was carried out using model-2 to -7, and the determined parameters for mixture-A and single mode are given in Table 3. The calculated parameters for mixture-B and mixture-C are given in Table 4. For the most part, the k values estimated through different models suggested that *p*-xylene oxidation rate is higher than toluene while toluene exhibited higher oxidation rate than benzene. It is interesting to note that model-6 could not fit to the experimental data, which assume that the reaction occurs in the gas phase. Thus, it can be concluded that the degradation of the target VOCs primarily occurred on the catalyst surface. The models-4, -5, and -7 fit well to the experimental degradation data. Generally, the models which give the good RSS and R^2 values are anticipated as the most probable kinetic path followed by a particular reaction. However, due to close values, we consider model-4, -5, and -7 (except for mixture-B) as the best fit models. The comparative analysis of these models suggested that adsorption equilibrium constant of water (K_W) is smaller than adsorption equilibrium constant of VOCs (K_A). Thus, it can be inferred that VOCs adsorbed more easily on the catalyst surface than water. This behavior has been explained in different studies, which reported that the photodegradation activity decreases with increasing relative humidity (RH) up to a certain level [39] and references therein. The low water content has been found to promote the PCO reaction. The photoinduced holes will oxidize the adsorbed water molecules to produce hydroxyl radicals. These •OH radicals act as an oxidizing agent in the PCO reaction. However, when the %RH increases to a certain level, the PCO might be affected negatively. First, the water molecules will cover some of the active surface sites, e.g., Ti^{4+} in TiO_2 [40]. Another possibility is the formation of a film of water molecules on a catalyst surface, which can hinder the physical interaction between the VOCs and catalysts [41]. The relative behavior between predicted rates vs. experimental rates determined through selective model-4, -5 (Fig. 5) and model-7 (Fig. S5) are given. It can be seen that the predicted values are in good agreement with the experimental values, which confirms the reliability of the implemented models.

3.3. *In situ FTIR study*

The real time analysis of a catalyst surface species during a photodegradation reaction using in-situ FTIR provide useful information about the intermediate's formation and mechanism of oxidation. The in-situ FTIR study was carried out for the mixture-A and VOCs in the isolated mode. The in-situ FTIR spectra of VOCs during adsorption process are given in Fig. S6. Due to a similar type of molecular structure, the absorption spectra of benzene, toluene, and *p*-xylene followed a somewhat similar pattern. The final FTIR spectra before starting the light is given for comparison in Fig. S7, which shows a progressive increase in intensity from benzene to *p*-xylene. Major peaks in the in-situ FTIR absorption spectra of mixture-A are identified for clarity. The peaks around 1635 cm^{-1} and 1602 cm^{-1} are associated with the aromatic ring vibration. After adsorption in the dark, the samples were irradiated. Different peaks were observed in all of the samples, including the mixture-A, which are associated with the presence of different species formed/adsorbed on the catalyst surface (Fig. 6). A summary of assigned IR modes to different functional groups is given in Table S1. These peaks are distinguished based on different reports [42,43,44,45,46,47,48,49]. The split peaks around the 2320 cm^{-1} and 2363 cm^{-1} are associated with CO_2 (Fig. 6b). These peaks are more pronounced in toluene (Fig. 6c) and *p*-xylene (Fig. 6d) contrasted to benzene spectra. Also, the intensity of CO_2 formation increased with increasing reaction time suggesting the ease of mineralization (complete oxidation) of toluene and *p*-xylene in contrast to benzene. This behavior is in good agreement with the degradation experiment, where benzene showed poor degradation efficiency than toluene and *p*-xylene. The peaks at 2734, 2843, 2907, and 2952 cm^{-1} are associated with C–H vibration. The peaks beyond 3680 cm^{-1} are associated with hydroxyl groups attached to Ti (linear; Ti–OH), while the peaks below 3680 cm^{-1} are associated with bridged hydroxyl groups (Ti–OH–Ti). The broad peak around 3200 cm^{-1} is due to adsorbed water molecules. These peaks are observed to increase, which is due to the regeneration of hydroxyl groups and their subsequent adsorption on the catalyst surface. Interestingly, the linear and bridged hydroxyl peaks in benzene and toluene are more complex, than *p*-xylene. The linear Ti-OH group in benzene appears at 3701 cm^{-1}. A similar kind of peak appears in toluene at 3691 cm^{-1} accompanied by a shoulder peak at 3741 cm^{-1}. In *p*-xylene FTIR spectra (Fig. 6d), a peak

Table 2
Rate and adsorption constant for different VOCs when water is not present.

Mixture-A					Single mode			
	k (ppmv min^{-1})	K_A ($ppmv^{-1}$)	*RSS*	R^2	k (ppmv min^{-1})	K_A ($ppmv^{-1}$)	*RSS*	R^2
Benzene	0.0095	0.2421	8.76×10^{-7}	0.94	0.0233	0.0717	1.75×10^{-4}	0.93
Toluene	0.0392	0.3921	9.81×10^{-5}	0.87	0.0845	0.2669	5.01×10^{-4}	0.84
p-xylene	0.0634	0.8434	9.06×10^{-5}	0.92	0.0949	0.2994	2.46×10^{-4}	0.87
Mixture-B								
Benzene	0.0337	0.0533	5.98×10^{-5}	0.73				
p-xylene	0.0625	1.4373	1.65×10^{-5}	0.96				
Mixture-C								
Benzene	0.0207	0.4236	2.58×10^{-5}	0.85				
toluene	0.0547	1.0008	4.82×10^{-5}	0.91				

Table 3
Rate and adsorption equilibrium constant of VOCs and water in the case of mixture-A and isolated mode when water is present.

L-H kinetic models						
	Model 2	*Model 3*	*Model 4*	*Model 5*	*Model 6*	*Model 7*
Mixture-A						
Benzene k	0.0045	0.0073	0.0085	0.0105	0.0411	0.0267
K_A	0.4724	1.5518	0.7181	0.2987	9.2814	0.3077
K_W	0.00018	0.00029	0.00005	0.0005	0.000001	0.00022
RSS	3.37×10^{-6}	3.34×10^{-6}	1.24×10^{-6}	1.24×10^{-6}	1.57×10^{-5}	7.96×10^{-7}
R^2	0.83	0.82	0.93	0.93	0.16	0.95
Toluenek	0.0242	0.0424	0.04128	0.1306	0.0605	0.0720
K_A	0.3471	0.8994	1.02159	0.3471	0.0594	0.6802
K_W	0.00019	0.0002	0.00004	0.00005	34.4498	0.00015
RSS	8.49×10^{-5}	8.00×10^{-5}	8.49×10^{-5}	8.49×10^{-5}	6.16×10^{-4}	5.09×10^{-5}
R^2	0.90	0.90	0.90	0.90	0.14	0.95
p-xylenek	0.3818	0.0107	0.066	0.8413	0.2886	0.1269
K_A	0.7443	1.5154	0.0559	1.4327	0.0245	2.6616
K_W	0.00002	0.00085	0.0015	0.00093	8.3922	0.00199
RSS	6.29×10^{-5}	1.92×10^{-6}	6.29×10^{-5}	1.85×10^{-6}	0.00349	2.12×10^{-5}
R^2	0.94	0.93	0.94	0.99	0	0.98
Single mode						
Benzenek	0.0164	0.1742	0.1662	0.427	0.1639	0.3021
K_A	0.0189	0.7732	0.0290	0.0184	0.1639	0.1055
K_W	0.0016	0.0031	0.00012	0.00067	0.00008	0.00109
RSS	1.24×10^{-4}	1.42×10^{-4}	8.35×10^{-5}	1.24×10^{-4}	1.43×10^{-4}	1.23×10^{-4}
R^2	0.95	0.93	0.97	0.88	0.76	0.96
Toluenek	0.4306	0.0818	0.0845	0.2744	0.2002	0.4281
K_A	0.2670	0.9130	0.1737	0.3548	0.0360	0.2316
K_W	0.000022	0.00025	0.00017	0.000045	0.0277	0.000089
RSS	5.01×10^{-4}	5.42×10^{-4}	5.01×10^{-4}	3.49×10^{-4}	0.00233	3.92×10^{-4}
R^2	0.86	0.84	0.86	0.87	0.27	0.91
p-xylenek	2.2201	0.0949	0.0949	0.9881	1.3159	0.0093
K_A	0.278	1.0281	0.9201	0.2997	0.3736	0.2211
K_W	0.000005	0.00027	0.00004	0.000012	0.000013	0.00002
RSS	2.65×10^{-4}	2.46×10^{-4}	2.46×10^{-4}	2.46×10^{-4}	0.0011	2.02×10^{-4}
R^2	0.88	0.89	0.89	0.89	0.45	0.92

Table 4
Rate and adsorption equilibrium constant of VOCs and water in the case of mixture-B and mixture-C when water is present.

L-H kinetic models						
	Model 2	*Model 3*	*Model 4*	*Model 5*	*Model 6*	*Model 7*
Mixture-B						
Benzene						
k	0.0047	0.0267	0.0235	0.0309	0.03521	0.0288
K_A	0.0343	0.3239	0.2085	0.0991	2.1234	0.7099
K_W	0.0011	0.0003	0.00006	0.00042	0.000009	0.00122
RSS	2.38×10^{-5}	6.44×10^{-5}	1.68×10^{-6}	6.88×10^{-5}	6.22×10^{-5}	7.63×10^{-5}
R^2	0.88	0.74	0.96	0.72	0.68	0.71
p-xylene						
k	0.1662	0.0608	0.0606	0.6052	0.0258	0.4077
K_A	1.4895	2.8671	0.5391	1.5412	0.2567	0.4749
K_W	0.00004	0.000098	0.00033	0.000013	0.00059	0.000093
RSS	5.08×10^{-5}	5.05×10^{-5}	4.97×10^{-5}	3.45×10^{-5}	0.00476	1.33×10^{-4}
R^2	0.89	0.89	0.88	0.93	0	0.85
Mixture-C						
Benzene						
k	0.0484	0.0206	0.0218	0.0273	0.0427	0.0413
K_A	0.4234	0.4174	0.0067	0.4235	0.0427	1.0349
K_W	0.00005	0.0094	0.0066	0.00035	0.4016	0.00089
RSS	2.58×10^{-5}	2.58×10^{-5}	2.62×10^{-5}	2.59×10^{-5}	2.41×10^{-4}	1.67×10^{-5}
R^2	0.87	0.86	0.87	0.87	0.0	0.93
Toluene						
k	0.1592	0.0547	0.0556	0.1626	0.4075	0.18645
K_A	1.0011	1.7714	1.5352	0.9428	0.01645	0.65877
K_W	0.00004	0.00009	0.00031	0.000059	0.0.00215	0.00025
RSS	4.83×10^{-5}	4.82×10^{-5}	4.01×10^{-5}	4.01×10^{-5}	0.00238	8.84×10^{-5}
R^2	0.92	0.91	0.92	0.93	0	0.86

gradually appears at 3710 cm^{-1}, which suggests the formation of OH species. It means that *p*-xylene did not entirely consume the OH species. A gradual formation during the course of the reaction suggests that initially the OH species were consumed faster. As the reaction progress, the appearance might be associated with the new OH species accumulated on TiO_2 surface. This small variation in the absorption bands of Ti–OH suggested different coordination environments in the case of benzene, toluene, and *p*-xylene. This behavior might be associated with two factors. First, the adsorption behavior of these VOCs is different, thus, the available adsorption sites and surface polarity due to

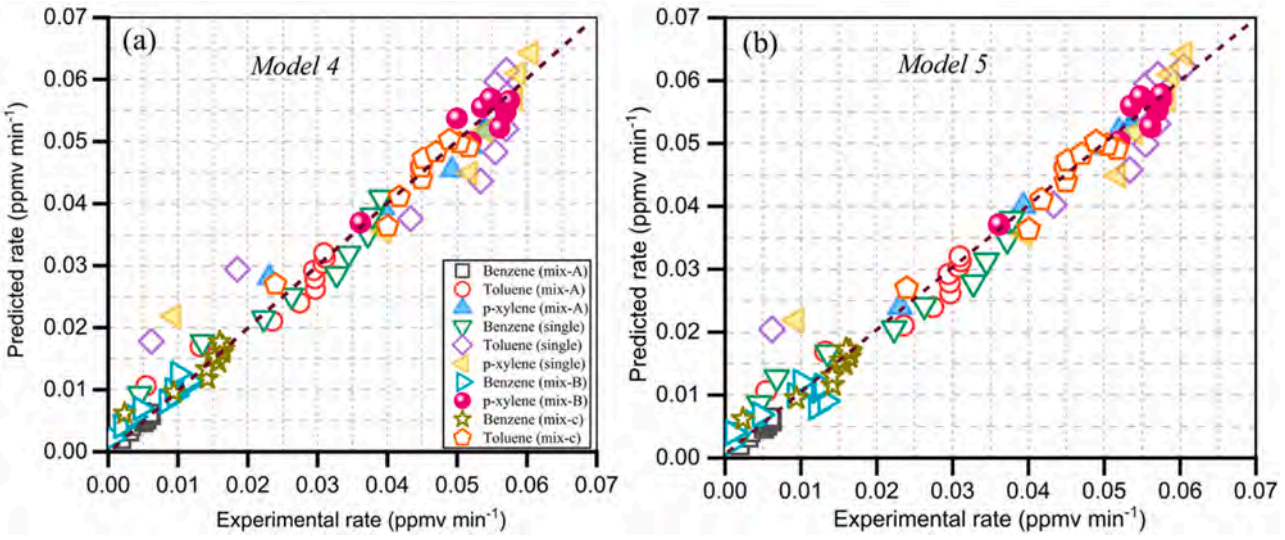

Fig. 5. Model 4 and 5 predicted reaction rates vs. experimental rates.

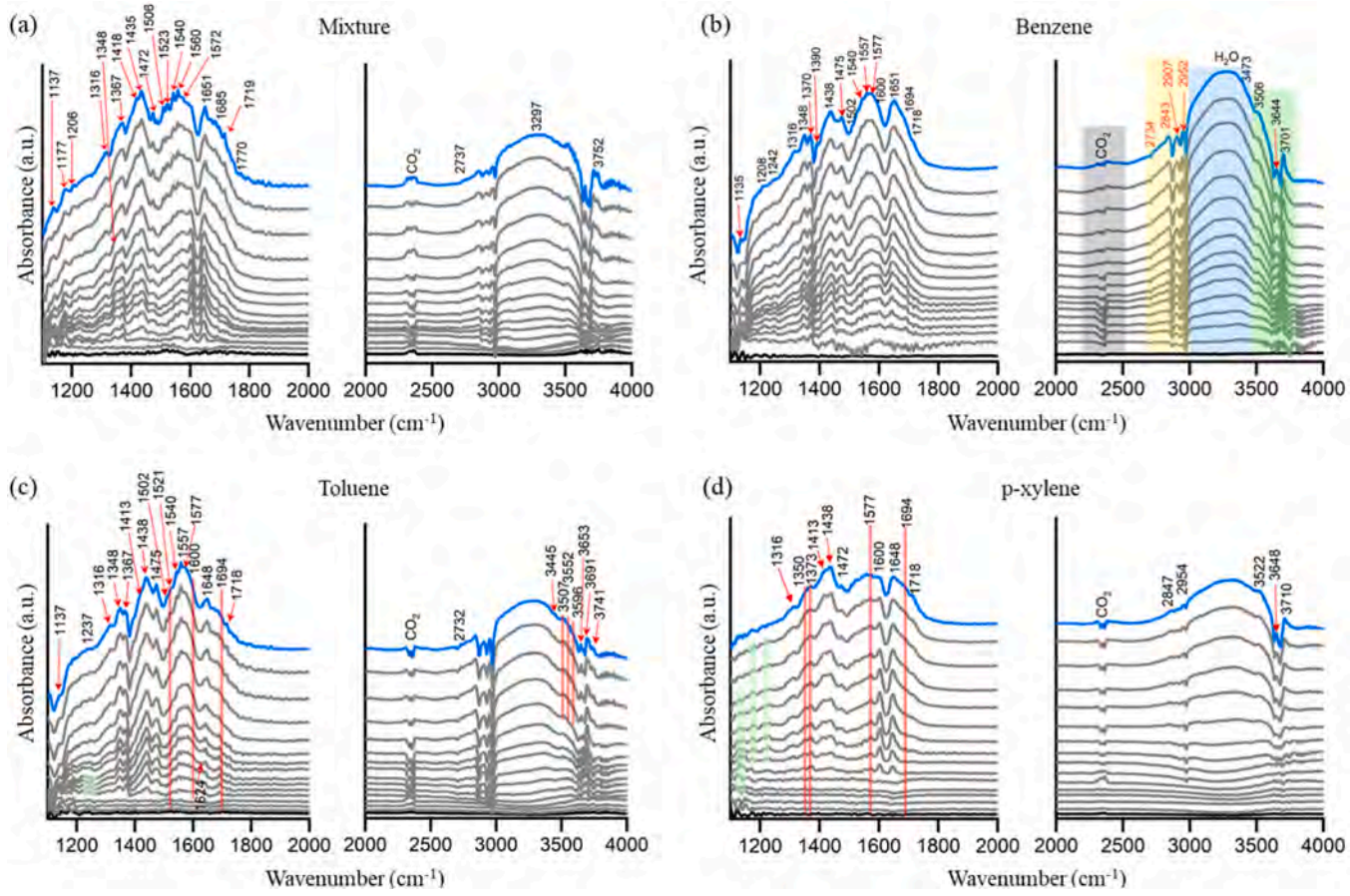

Fig. 6. In-situ FTIR spectra of benzene toluene, and *p*-xylene in mixture-A and isolated mode under UV–vis light irradiation. The time interval for FTIR spectrum is 3 min.

these molecules would vary accordingly. Therefore, the interaction of hydroxyl radicals due to adsorption and formation with TiO_2 will be different. Second, the fragment formation (intermediates) in the case of different VOCs is anticipated different. A similar behavior was observed for the bridged Ti–OH–Ti species, which shows different coordination environment. Also, the relative abundance of these species is low in the case of *p*-xylene than benzene and toluene, suggesting that linear Ti–OH groups are utilized quickly during the photodegradation reaction of *p*-xylene. Hennezel et al. [50] reported that the degradation of benzene might follow two routes, (a) direct oxidation by a photoinduced hole, (b) or through the surface hydroxyl radicals. The direct oxidation reaction could generate benzene radicals, which can further react and polymerize benzene species on TiO_2 surface. In contrast, the polymerization process could be suppressed through the •OH radical's route. However, it is

quite hard to predict the specific species and their role in such a complex system involving different reactions at the same time. The broad peak around 3297 cm^{-1} is due to adsorbed water molecules. Also, in benzene and toluene small band around the 1624 cm^{-1} could be seen, which is associated with the bending vibration of adsorbed water molecules. This peak could not be detected in *p*-xylene. The results revealed by in situ FTIR confirmed our speculations about the robust •OH radicals' consumption in the case of *p*-xylene than benzene and toluene. In addition to adsorption, this could be the possible reason that *p*-xylene exhibit a high photodegradation efficiency while the presence of *p*-xylene in the mixture-A and mixture-B suppressed the benzene/toluene and benzene degradation, respectively. The small peak at 1718 cm^{-1} is associated with the adsorbed benzaldehyde. The peak at 1694 cm^{-1} is related to C=O stretching vibration of aldehyde groups. The bands at 1600 cm^{-1} and 1577 cm^{-1} are attributed to C=C and C–C stretching vibration of the aromatic ring, respectively. The peak at 1540 cm^{-1} is due to antisymmetric C–O stretching vibration of benzoate, while the peak at 1502 cm^{-1} is attributed to C–C skeletal vibration of aromatic rings. The peak at 1716 cm^{-1} is due to aliphatic groups while several peaks beyond this range (1786–1846 cm^{-1}) are due to C=O groups which can be associated with the cracking of aromatic rings. The small peak at 1316 cm^{-1} is due to weakly adsorbed aromatic aldehyde groups. The shoulder peak at 1413 cm^{-1} is due to the interaction of C–O and OH of carboxylate species. If we compare the in-situ results under light illumination, the following conclusion can be inferred.

(a) *p*-xylene adsorb more on TiO_2 P25 than benzene and toluene.
(b) *p*-xylene exhibit high mineralization efficiency than benzene and toluene.
(c) The hydroxyl radicals are readily utilized by *p*-xylene, which will eventually influence the conversion efficiency of benzene and toluene.
(d) The fundamental difference in these molecules is the end group (methyl group) attached to the aromatic ring, which affects the adsorption and ease of reaction on TiO_2 surface.

The photodegradation, in-situ FTIR and DFT results can be used to anticipate the degradation mechanism of benzene, toluene, and *p*-xylene. Although, it is not possible to determine the exact path followed by these VOCs in the current experimental setup, still an overall degradation route can be anticipated. A schematic view of the proposed mechanism is given in Fig. 7. As stated earlier, for the gas-solid reactions, the adsorption of a particular VOC is critical. Thus, the VOCs are first adsorbed on TiO_2 P25 nanoparticles. The kinetic analysis and calculated values of K_A and K_W suggested that VOCs adsorbed easily on TiO_2 P25 than water content. Also, the implementation of L-H models to experimental data suggested that the oxidation reactions occurred on the catalyst surface (at least for the most part) and not in the gas-phase. The adsorption energy values calculated through DFT suggested that *p*-xylene strongly interacted with TiO_2 (101) surface, which exhibited a high adsorption energy value (0.767 eV). In contrast, toluene (0.597 eV) and benzene (0.541 eV) showed poor interaction with the TiO_2 (101) surface. Thus, it was seen that *p*-xylene degraded more in contrast to benzene and toluene. The in-situ FTIR results revealed that the degradation of VOCs is followed by several intermediate steps. Adsorption of pollutant molecules is a crucial step in gas-solid heterogeneous catalysis. Initially, the VOCs molecules e.g., benzene, toluene, and p-xylene will adsorb on TiO_2 P25 surface. When the catalyst is irradiated within the UV–vis region, hole-electron pairs are generated. There are two possibilities for the surface catalyzed reaction in this scenario, which include, (a) a direct reaction between photoinduced holes and VOC molecules, (b) the photoinduced hole-electron will activate the surface adsorbed species to produce reactive oxygen species (ROSs) such as •OH and $\bullet O_2^-$ radicals. These ROSs further take part in the photodegradation of VOCs. The in-situ FTIR results suggested that several rings containing species are formed as a result of this first interaction. Next, the ring containing species will be further converted into several small and long open chain intermediate species, which will be ultimately mineralized. The results further suggested that several intermediate species are stable on the catalyst surface and thus incomplete oxidation occurred in the case of aromatic ring containing VOCs.

4. Conclusion

In summary, the photodegradation of gas phase benzene, toluene, and *p*-xylene was studied on TiO_2 P25. The experimental results were analyzed through several Langmuir-Hinshelwood kinetic models, which provide a comprehensive picture of gas-solid reaction. The VOCs behave quite differently in the mixture when compared with isolated mode. For example, when benzene was degraded with toluene and *p*-xylene, a low degradation efficiency was achieved for benzene (10%). However, a high degradation efficiency (67%) was achieved in isolated mode. In the mixture of benzene and *p*-xylene, 20% of benzene was degraded. When *p*-xylene was used in the mixture instead of toluene, 27% of degradation efficiency was achieved for benzene. Thus, it can be inferred that *p*-xylene influences more the degradation of benzene than toluene. Similarly, the degradation efficiencies of toluene and *p*-xylene changed significantly when used in the mixture and isolated mode. The DFT results further revealed that the interaction of VOCs with TiO_2 (101) surface increases to a greater extent when the TiO_2 (101) surface was incorporated an oxygen vacancy. Therefore, the surface vacancies will play a significant role for better capture of VOCs. The in-situ FTIR results revealed that the degradation is followed by several intermediate steps. The high degradation rate of *p*-xylene could be associated with its chemical structure, which contains two methyl groups attached to an aromatic ring and strong affinity towards the catalyst surface. This study

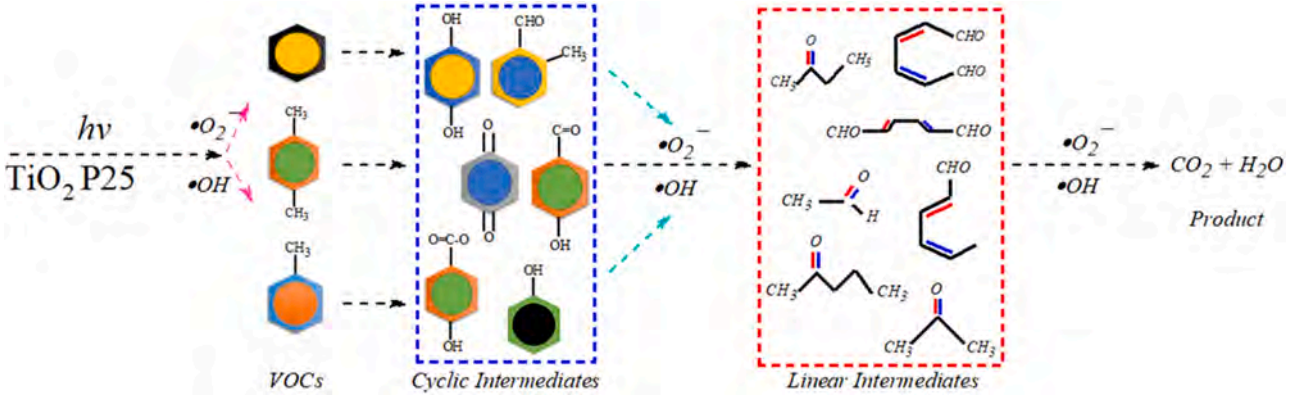

Fig. 7. A schematic view of the degradation pathways followed by benzene, toluene, and *p*-xylene on commercial TiO_2 P25.

is useful in understanding the reactivity of VOCs in the mixture and isolated mode, their comparative kinetics, role of moisture content, and degradation behavior, which can be exploited to manipulate the materials and engineering perspectives for designing an oxidation reactor.

CRediT authorship contribution statement

Asad Mahmood: Conceptualization, Methodology, Formal analysis, Data curation, Funding acquisition, Writing-original draft. **Wang Xiao**: Data curation, Formal analysis, Funding acquisition. **Xiaofeng Xie**: Investigation, Validation, Funding acquisition, Resources, Project administration. **Jing Sun**: Conceptualization, Methodology, Resources, Funding acquisition, Supervision, Project administration, Validation, Writing-review & editing.

Declaration of Competing Interest

The authors declare no competing financial interest.

Acknowledgment

This work was financially supported by the National Key Research and Development Program of China (2016YFA0203000), Shanghai Commission of Science and Technology Program (19DZ1202600, 20DZ1204100), the National Natural Science Foundation of China (Grant No. 41907303), and the Innovation Fund of SICCAS (No. Y91ZC5150G).

Appendix A. Supporting information

Supplementary data associated with this article can be found in the online version at doi:10.1016/j.jece.2021.105069.

References

[1] AFNOR (Association Française de Normalisation), XP B44–013 – Photocatalysis – Test and Analysis Method for Determining the Efficacy of Photocatalytic Systems for Eliminating Volatile Organic Compounds/odours in Recirculating Interior Air – Confined Chamber Test, 2009.
[2] H. Chen, C.E. Nanayakkara, V.H. Grassian, Titanium dioxide photocatalysis in atmospheric chemistry, Chem. Rev. 112 (11) (2012) 5919–5948.
[3] O. Debono, V. Hequet, L. Le Coq, N. Locoge, F. Thevenet, VOC ternary mixture effect on ppb level photocatalytic oxidation: removal kinetic, reaction intermediates and mineralization, Appl. Catal. B Environ. 218 (2017) 359–369.
[4] Faisal I. Khan, A.K. Ghoshal, Removal of volatile organic compounds from polluted air, J. Loss Prev. Process Ind. 13 (2000) 527–545.
[5] G. Kresse, J. Furthmuller, Efficiency of ab-initio total energy calculations for metals and semiconductors using a plane-wave basis set, Comput. Mater. Sci. 6 (1996) 15–50.
[6] V. Gombac, L. De Rogatis, A. Gasparotto, G. Vicario, T. Montini, D. Barreca, G. Balducci, P. Fornasiero, E. Tondello, M. Graziani, TiO_2 nanopowders doped with boron and nitrogen for photocatalytic applications, Chem. Phys. 339 (1–3) (2007) 111–123.
[7] S. Grimme, Semiempirical GGA-type density functional constructed with a long-range dispersion correction, J. Comput. Chem. 27 (15) (2006) 1787–1799.
[8] Y. Guo, D.-P. Yang, M. Liu, X. Zhang, Y. Chen, J. Huang, Q. Li, R. Luque, Enhanced catalytic benzene oxidation over a novel waste-derived Ag/eggshell catalyst, J. Mater. Chem. A 7 (15) (2019) 8832–8844.
[9] B. Hauchecorne, T. Tytgat, S.W. Verbruggen, D. Hauchecorne, D. Terrens, M. Smits, K. Vinken, S. Lenaerts, Photocatalytic degradation of ethylene: an FTIR in situ study under atmospheric conditions, Appl. Catal. B Environ. 105 (1–2) (2011) 111–116.
[10] V. Héquet, C. Raillard, O. Debono, F. Thévenet, N. Locoge, L. Le Coq, Photocatalytic oxidation of VOCs at ppb level using a closed-loop reactor: the mixture effect, Appl. Catal. B Environ. 226 (2018) 473–486.
[11] K. Hu, K.C. Robson, E.E. Beauvilliers, E. Schott, X. Zarate, R. Arratia-Perez, C. P. Berlinguette, G.J. Meyer, Intramolecular and lateral intermolecular hole transfer at the sensitized TiO_2 interface, J. Am. Chem. Soc. 136 (3) (2014) 1034–1046.
[12] G. Huang, S. Li, L. Liu, L. Zhu, Q. Wang, Ti_3C_2 MXene-modified Bi_2WO_6 nanoplates for efficient photodegradation of volatile organic compounds, Appl. Surf. Sci. 503 (2020), 144183.
[13] John P. Perdew, Kieron Burke, M. Ernzerhof, Generalized gradient approximation made simple, Phys. Rev. Lett. 77 (1996) 3865–3868.
[14] J. Kim, B.-K. Lee, Enhanced photocatalytic decomposition of VOCs by visible-driven photocatalyst combined Cu-TiO_2 and activated carbon fiber, Process Saf. Environ. Prot. 119 (2018) 164–171.
[15] C.A. Korologos, C.J. Philippopoulos, S.G. Poulopoulos, The effect of water presence on the photocatalytic oxidation of benzene, toluene, ethylbenzene and m-xylene in the gas-phase, Atmos. Environ. 45 (39) (2011) 7089–7095.
[16] G. Kresse, J. Furthmuller, Efficient iterative schemes for ab initio total-energy calculations using a plane-wave basis set. Phys. Rev. B 54 (1996) 169–186.
[17] G. Kresse, J. Hafner, Ab initiomolecular dynamics for liquid metals, Phys. Rev. B 47 (1) (1993) 558–561.
[18] P. Li, S. Kim, J. Jin, H.C. Do, J.H. Park, Efficient photodegradation of volatile organic compounds by iron-based metal-organic frameworks with high adsorption capacity, Appl. Catal. B Environ. 263 (2020), 118284.
[19] Y.-H. Lin, H.-T. Hsueh, C.-W. Chang, H. Chu, The visible light-driven photodegradation of dimethyl sulfide on S-doped TiO_2: Characterization, kinetics, and reaction pathways, Appl. Catal. B Environ. 199 (2016) 1–10.
[20] C. Liu, X. Zhang, Q. Wang, K. Shi, Role of PM2.5 in the photodegradation of the atmospheric benzene, Environ. Pollut. 247 (2019) 447–456.
[21] H. Liu, Y. Ma, J. Chen, M. Wen, G. Li, T. An, Highly efficient visible-light-driven photocatalytic degradation of VOCs by CO_2-assisted synthesized mesoporous carbon confined mixed-phase TiO_2 nanocomposites derived from MOFs, Appl. Catal. B Environ. 250 (2019) 337–346.
[22] R. Liu, H. Song, B. Li, X. Li, T. Zhu, Simultaneous removal of toluene and styrene by non-thermal plasma-catalysis: effect of VOCs interaction and system configuration, Chemosphere 263 (2021), 127893.
[23] X. Liu, Y. Zhang, S. Matsushima, H. Hojo, H. Einaga, Photocatalytic oxidation process for treatment of gas phase benzene using Ti^{3+} self-doped TiO_2 microsphere with sea urchin-like structure, Chem. Eng. J. 402 (2020), 126220.
[24] A. Mahmood, G. Shi, Z. Wang, Z. Rao, W. Xiao, X. Xie, J. Sun, Carbon quantum dots-TiO_2 nanocomposite as an efficient photocatalyst for the photodegradation of aromatic ring-containing mixed VOCs: an experimental and DFT studies of adsorption and electronic structure of the interface, J. Hazard. Mater. 401 (2021), 123402.
[25] A. Mahmood, G. Shi, X. Xie, J. Sun, Adsorption mechanism of typical oxygen, sulfur, and chlorine containing VOCs on TiO_2 (001) surface: first principle calculations, Appl. Surf. Sci. 471 (2019) 222–230.
[26] A. Mahmood, G. Shi, X. Xie, J. Sun, Assessing the adsorption and photocatalytic activity of TiO_2 nanoparticles for the gas phase acetaldehyde: a computational and experimental study, J. Alloy. Compd. 819 (2020), 153055.
[27] A.J. Maira, J.M. Coronado, V. Augugliaro, K.L. Yeung, J.C. Conesa, J. Soria, Fourier transform infrared study of the performance of nanostructured TiO_2 particles for the photocatalytic oxidation of gaseous toluene, J. Catal. 202 (2) (2001) 413–420.
[28] A.H. Mamaghani, F. Haghighat, C.-S. Lee, Gas phase adsorption of volatile organic compounds onto titanium dioxide photocatalysts, Chem. Eng. J. 337 (2018) 60–73.
[29] A.H. Mamaghani, F. Haghighat, C.-S. Lee, Photocatalytic degradation of VOCs on various commercial titanium dioxides: Impact of operating parameters on removal efficiency and by-products generation, Build. Environ. 138 (2018) 275–282.
[30] G. Marci, M. Addamo, V. Augugliaro, S. Coluccia, E. García-López, V. Loddo, G. Martra, L. Palmisano, M. Schiavello, Photocatalytic oxidation of toluene on irradiated TiO_2: comparison of degradation performance in humidified air, in water and in water containing a zwitterionic surfactant, J. Photochem. Photobiol. A Chem. 160 (1–2) (2003) 105–114.
[31] Olga d'Hennezel, Pierre Pichat, D.F. Ollis, Benzene and toluene gas-phase photocatalytic degradation over H_2O and HCL pretreated TiO_2: by-products and mechanisms, J. Photochem. Photobiol. A Chem. 118 (1998) 197–204.
[32] N. Quici, M.L. Vera, H. Choi, G.L. Puma, D.D. Dionysiou, M.I. Litter, H. Destaillats, Effect of key parameters on the photocatalytic oxidation of toluene at low concentrations in air under 254+185nm UV irradiation, Appl. Catal. B Environ. 95 (3–4) (2010) 312–319.
[33] Rafael Méndez-Román, N. Cardona-Martínez, Relationship between the formation of surface species and catalyst deactivation during the gas-phase photocatalytic oxidation of toluene, Catal. Today 40 (1998) 353–365.
[34] Z. Rao, G. Shi, Z. Wang, A. Mahmood, X. Xie, J. Sun, Photocatalytic degradation of gaseous VOCs over Tm^{3+}-TiO_2: Revealing the activity enhancement mechanism and different reaction paths, Chem. Eng. J. 395 (2020), 125078.
[35] Z. Rui, M. Tang, W. Ji, J. Ding, H. Ji, Insight into the enhanced performance of TiO_2 nanotube supported Pt catalyst for toluene oxidation, Catal. Today 297 (2017) 159–166.
[36] S. Ardizzone, C.L. Bianchi, G. Cappelletti, A. Naldoni, C. Pirola, Photocatalytic degradation of toluene in the gas phase: relationship between surface species and catalyst features, Environ. Sci. Technol. 42 (2008) 6671–6676.
[37] P.N. Samanta, D. Majumdar, S. Roszak, J. Leszczynski, First-principles approach for assessing cold electron injection efficiency of dye-sensitized solar cell: elucidation of mechanism of charge injection and recombination, J. Phys. Chem. C 124 (5) (2020) 2817–2836.
[38] Z. Shayegan, F. Haghighat, C.-S. Lee, Carbon-doped TiO_2 film to enhance visible and UV light photocatalytic degradation of indoor environment volatile organic compounds, J. Environ. Chem. Eng. 8 (5) (2020), 104162.
[39] G. Shi, A. Mahmood, G. Lu, X. Wang, S. Tong, M. Ge, X. Xie, J. Sun, Adsorption and photodegradation of acetaldehyde and ethylene on TiO_2 (001) Surface: experimental and first principle studies, Catal. Lett. 149 (2019) 2728–2738.
[40] M. Stucchi, F. Galli, C.L. Bianchi, C. Pirola, D.C. Boffito, F. Biasioli, V. Capucci, Simultaneous photodegradation of VOC mixture by TiO_2 powders, Chemosphere 193 (2018) 198–206.
[41] M. Sun, X. Wang, Z. Chen, M. Murugananthan, Y. Chen, Y. Zhang, Stabilized oxygen vacancies over heterojunction for highly efficient and exceptionally

durable VOCs photocatalytic degradation, Appl. Catal. B Environ. 273 (2020), 119061.
[42] J. Sundell, On the history of indoor air quality and health, Indoor Air 14 (2004) 51–58.
[43] Z. Wang, X. Xie, X. Wang, A. Mahmood, H. Qiu, J. Sun, Difference of photodegradation characteristics between single and mixed VOC pollutants under simulated sunlight irradiation, J. Photochem. Photobiol. A Chem. 384 (2019), 112029.
[44] M. Wen, G. Li, H. Liu, J. Chen, T. An, H. Yamashita, Metal–organic framework-based nanomaterials for adsorption and photocatalytic degradation of gaseous pollutants: recent progress and challenges, Environ. Sci. Nano 6 (4) (2019) 1006–1025.
[45] M. Woellner, S. Hausdorf, N. Klein, P. Mueller, M.W. Smith, S. Kaskel, Adsorption and detection of hazardous trace gases by metal-organic frameworks, Adv. Mater. 30 (37) (2018), 1704679.
[46] F. Zhang, M. Wang, X. Zhu, B. Hong, W. Wang, Z. Qi, W. Xie, J. Ding, J. Bao, S. Sun, C. Gao, Effect of surface modification with H_2S and NH_3 on TiO_2 for adsorption and photocatalytic degradation of gaseous toluene, Appl. Catal. B Environ. 170–171 (2015) 215–224.
[47] H. Zhou, Z. Wen, J. Liu, J. Ke, X. Duan, S. Wang, Z-scheme plasmonic Ag decorated WO_3/Bi_2WO_6 hybrids for enhanced photocatalytic abatement of chlorinated-VOCs under solar light irradiation, Appl. Catal. B Environ. 242 (2019) 76–84.
[48] Z. Zhu, X. Li, Q. Zhao, Z. Qu, Y. Hou, L. Zhao, S. Liu, G. Chen, FTIR study of the photocatalytic degradation of gaseous benzene over UV-irradiated TiO_2 nanoballs synthesized by hydrothermal treatment in alkaline solution, Mater. Res. Bull. 45 (12) (2010) 1889–1893.
[49] P.J. Ziemann, R. Atkinson, Kinetics, products, and mechanisms of secondary organic aerosol formation, Chem. Soc. Rev. 41 (19) (2012) 6582–6605.
[50] W. Zou, B. Gao, Y.S. Ok, L. Dong, Integrated adsorption and photocatalytic degradation of volatile organic compounds (VOCs) using carbon-based nanocomposites: a critical review, Chemosphere 218 (2019) 845–859.